Escola de Primavera de Transição e Turbulência
Blumenau 2022

ABCM
13th Spring School on Transition and Turbulence
September 19th-23rd, 2022, Blumenau, SC, Brazil

EPTT-2022-0067
Comparison of wake effects on wind turbines operating in complex terrain varying the free stream turbulence

Victor Couto Durra
Bruno Souza Carmo
Department of Mechanical Engineering – Escola Politécnica, University of São Paulo
victordurra@usp.br, bruno.carmo@usp.br

Abstract. *Due to the increase of interest in wind energy, complex terrains have become fundamental to its expansion. Through Computational Fluid Dynamics (CFD) simulations, in an idealized complex terrain (slope and plain), this paper presents a comparison of two inflow types in the developed numerical domain: laminar and synthetic turbulent Atmospheric Boundary Layer (ABL) inflows, which produces a logarithmic mean velocity profile. Regarding the turbulent inflow, the inlet type used is the Turbulence Divergence-Free Synthetic Method (DF-SEM), which is a velocity boundary condition that synthesizes eddies in Large Eddy Simulations (LES). It was possible to assess the wake effects in two NREL 5MW wind turbines in tandem as the inflow changes. This has been devised in the open-source software OpenFOAM, using the LES turbulence model and modelling the turbines with the Actuator Line Method (ALM). Power production during the simulations, power coefficient calculated using probes and turbulence parameters were employed to assess the simulation response. The obtained results showed that the turbulence influences the turbines' performance, specifically due to the faster wake recovery effect compared to the laminar counterpart.*

Keywords: *Wind turbine wakes, Complex terrain, Wake effect, Atmospheric turbulence, Computational simulation*

1. INTRODUCTION

Wind energy has received increasing attention from companies and governments because of its role in the energy transition. Due to a significant reduction of the cost of this energy in the last few years, reaching $0.04/kWh approximately, estimates show that this source will be able to produce from 25 to 33% of the global energy demand until 2050 (Veers *et al.*, 2019). According to the Global Wind Report 2022 (Lee and Zhao, 2022), despite the second year of the pandemic, in 2021, 93.6 GW have been added to the global capacity, a 12% growth compared to 2020, which had already been a record year. In 2021, Brazil represented 5% of the new and 3% of the total onshore installations.

As wind power generation disseminate around the world, locations considered ideal, with flat topography, high wind speeds and low turbulence are becoming more scarce (Alfredsson and Segalini, 2017). In order to overcome this problem, wind farms have been installed offshore, where properties similar to those previously reported are found. However, the high costs of installation and maintenance of turbines, and transmission of energy to the coast are economic obstacles. In view of this, another alternative that has been explored and that should increase in the near future is the installation of wind farms on complex terrains. Even though in these places there is predominance of lower speeds and greater turbulence, it is possible that profiles such as hills, mesas and ridges can present suitable wind regimes for the turbines (Sandusky, 2017).

In complex terrains, the definition of the wind speed conditions and of the atmospheric stability become more complicated due to the interaction with the terrain and because the turbines are located just above the atmospheric rough layer (Alfredsson and Segalini, 2017). An investigation about the wake effect in a set of four wind turbines located on an extremely complex terrain, using experimental data to calibrate the computational modeling, concluded that the wake effect in the case of a complex terrain is diminished compared to a flat terrain (Castellani *et al.*, 2017). This justifies the better energy production of the turbine further downstream that was found on the paper. It is noteworthy that, in the numerical simulation, a neutral boundary layer was considered and Reynolds-Average Navier-Stokes (RANS) model was used.

It is known that the mechanical turbulence is generated by the friction the surface exerts on the wind, which causes it to shear. According to Porté-Agel *et al.* (2020), situations where the turbulence is higher, such as those caused by the convective boundary layer, there is an increased turbulent mixture compared to the neutral boundary layer condition. Thus, the wake recovery is faster and the wind farm performance in the former situation is better.

In this paper, a simplified numerical model of a complex terrain in the state of Bahia is presented and several CFD Large Eddy Simulations (LES) are carried out in order to compare how a change in the inlet type may influence the wake effect on a downstream turbine of a tandem pair and its power production. Initially, two simulations with a laminar inlet type were performed. Subsequently, two simulations were carried using a synthetic turbulent inlet type. The results were compared assessing the power production, the power coefficient via probes located upstream from the turbines and turbulence parameters.

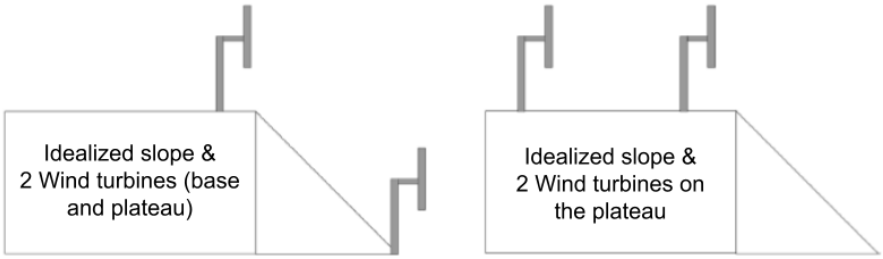

Figure 1: Turbine pair layouts used in the simulations.

2. METHODOLOGY

The open-source software OpenFOAM (OpenCFD, 2022) and the actuator line library turbinesFOAM (Bachant, 2019) were employed to conduct the LES simulations. The laminar simulations were performed on a workstation powered by two Intel Xeon X560 processors, 12 cores and 96 GB of RAM memory. The turbulent simulations were carried on a workstation which has two Intel Xeon e5-2680 processors, 16 cores and 48 GB of RAM memory. These two machines belong to the Fluids & Dynamics Research Group from the University of São Paulo.

Besides the two different inflow conditions, the turbines layout was also varied. As seen in Fig. 1, where the flow comes from right to left, the first disposition is with a turbine at the base of the slope and the downstream one located at the beginning of the plateau. In the second one, both turbines are on the plateau. In total, four simulations were carried out. Whilst two simulations had a default laminar inlet, which means the velocity at each point in the inlet is constant throughout the entire simulation, the other two had a synthetic turbulence inlet, called Divergence-Free Synthetic Method (DF-SEM) (OpenCFD, 2021), which is a velocity boundary condition that synthesizes eddies in Large Eddy Simulations (LES). This means for the latter inlet type that at each time step, the velocity at a certain point in the inlet has an oscillation that synthesizes free atmospheric turbulence.

Concerning the DF-SEM, it is paramount to explain the inlet configurations. The velocity was determined, for all the simulations, as being 10.59 m/s at the hub height of the turbine at the base of the slope. In order to generate this loglaw profile for the wind, simulating approximately the behavior of the Atmospheric Boundary Layer (ABL), different heights in the same vertical line located at the inlet coordinate were chosen. Then, a script was written to calculate these velocities at different heights, following the expressions

$$u = \frac{u^*}{\kappa} \ln\left(\frac{z - d + z_0}{z_0}\right), \qquad u^* = \frac{u_{ref}\kappa}{\ln\left(\frac{z_{ref}+z_0}{z_0}\right)} \tag{1}$$

and guaranteeing the desired velocity magnitude at the hub height. u the desired wind velocity in the flow direction, u^* the shear velocity, u_{ref} the reference velocity and z_{ref} the reference height, z the height considered for the calculation, d the height where the velocity is null and z_0 the terrain roughness. Both result files, with the points and the velocity magnitudes, are inputs for the simulation.

In the simulations carried for this paper, u_{ref} and z_{ref} are, respectively, 10.59 m/s and 90 m, d is equal to -90 m and $z_0 = 0.1$. At the inlet, only the horizontal velocity component has magnitude, while the others start at zero. Another parameter determined in this boundary condition is the Reynolds Stress Tensor that, due to simplification, was chosen to be uniform and constant. Regarding the other boundary conditions, on the bottom wall of the numerical domain, the floor, the velocity is zero and the pressure gradient in the normal direction is also zero. On the outlet, the velocity has a zero gradient and the pressure a fixed value. On the top, the upper wall, the pressure has a zero gradient and the velocity has a symmetric condition, with both normal velocity and normal gradient of tangential velocity null. Lastly, on both lateral walls, the boundary condition for the velocity is the same as the previous one and the pressure has a zero gradient.

Further detailing the numerical domain, for the simulations related to the layout on the left hand side of Fig. 1, the dimensions presented in the Fig. 2 are considered. The mesh comprised 3.4 million cells. The coordinates for this domain range from -720 to 2400 in the x direction, from -395 to 395 in the y direction and from -90 to 600 in the z direction (all lengths are in meters). For the second layout, the plateau dimension was further extended 600 m in the x direction, which added 1 million cells to the original configuration, so that the fluid flow could develop better downstream the second turbine and to prevent unintended numerical effects. In both situations, the fluid was set to flow up the slope in the domain. In the former disposition, the coordinates of the turbines were (290, 0, 0) and (1240, 0, 100), whilst in the latter the coordinates are (1240, 0, 100) and (1860, 0, 100).

The wind turbines used in the simulations were the NREL 5 MW (Jonkman *et al.*, 2009), which has a 90 m hub height and a blade length of 63 m. The simulations were carried only with the turbine's rotor (hub and blades), neglecting nacelle and tower effects. It is worth mentioning that these turbines neither have a rotor speed control nor a pitch control installed yet. Thus, some results are influenced by this.

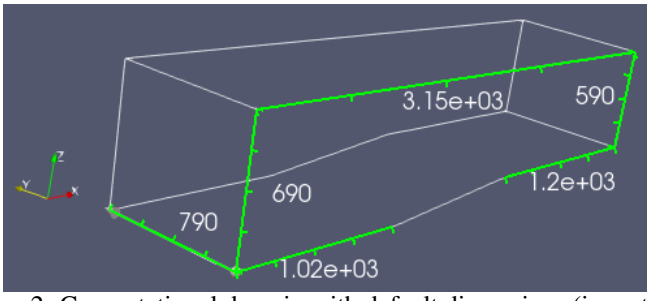

Figure 2: Computational domain with default dimensions (in meters).

All simulations were performed using the solver pimpleFoam, which is usually employed in turbulent and incompressible flows. The flow was simulated for 400 s and a time-step of 0.1 s was employed. The turbines were set to operate with a constant Tip Speed Ratio (TSR) of 7.55 (based on the inlet average speed at hub height) and considering the tip loss correction activated (Shen *et al.*, 2005).

The results analysed were the history of turbine power generation, as well as power coefficients and turbulence parameters. With respect to the first one, the turbinesFOAM library generates a csv file as an output of the simulation, which consists of several parameters calculated at each time-step, with the power coefficient among those. Using a script in python, it was possible to obtain the power production via

$$P = \frac{\rho_{air} C_p \pi R^2 U_\infty^3}{2}, \tag{2}$$

where ρ_{air} is the air density at 20 ºC, C_p is the power coefficient given as an output in each time-step, R is the blade radius and U_∞ is the free stream velocity at hub height.

Regarding the power coefficient, it is necessary to obtain the speed of the wind that reaches each turbine. For that reason, probes were placed on the rotor plane and one diameter upstream of all turbines. The axial wind speed one diameter upstream of the turbines was used as the free stream velocity in the expression of the axial induction factor a (Hansen, 2015),

$$a = \frac{U_\infty - U_{rotor}}{U_\infty}, \tag{3}$$

with the objective to capture more precisely how the flow evolves in the domain. Then, the power coefficient C_p is calculated, for each time-step, with

$$C_p = 4a(1-a)^2. \tag{4}$$

Two turbulence parameters were assessed: Turbulence Intensity (TI) and Turbulence Kinetic Energy (TKE). The former represents the intensity of the wind fluctuation at a specified point, considering one velocity component only, and is given by the standard deviation divided by the average and then indicated in percentage. The latter is also obtained at a specific point, and is obtained by adding the variances of all velocity components dividing by 2. These metrics will be used to compare the turbulence levels near the turbines as the inlet type and turbine arrangement are varied. In the simulations performed for this paper, this point is located one diameter upstream from the turbines.

3. RESULTS AND DISCUSSIONS

We start by defining the nomenclature and conventions that will be employed in the graphs and table of this section. Figure 1 shows both layouts considered in the simulations. In the left hand side one, the first turbine is named $P1$ (position 1) and the downstream one, $P3$ (position 3). In the right hand side one, the first turbine is still $P3$, but the second one is $P4$ (position 4).

It is important to clarify that these simulations were not performed with a precursor simulation to obtain an equilibrium state in the turbulence. Therefore, we cannot guarantee that the turbulence is fully developed in the atmospheric boundary layer. Nevertheless, the results presented in the tables were calculated disregarding the initial transient, considering the time series starting from the simulation time when the first turbine in each layout reaches a considerable stabilization, which can be seen in the figures to follow. For the layout with $P1$ and $P3$, this time is 90 s and for the one with $P3$ and $P4$, it is 160 s.

In first layout, where the turbines are located in the positions $P1$ and $P3$, it can be seen in Fig. 3, for the turbine in $P1$, with the laminar inlet, the power converges to a value near the rated power and with minimum oscillation. Conversely, with the turbulent inlet, the oscillation is much more intense, as expected, causing the power to deviate from the rated power. For the turbine in $P3$, the behaviour as the power decreases to reach the operating condition, as the flow upstream

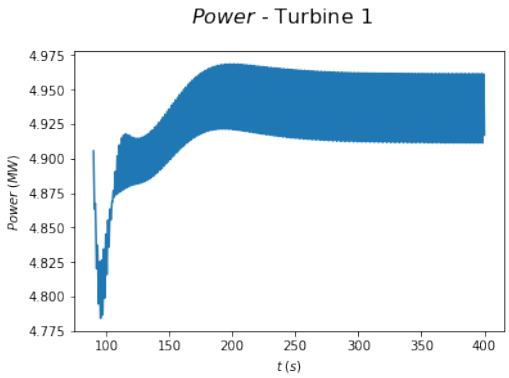

(a) Power for laminar inlet - P1

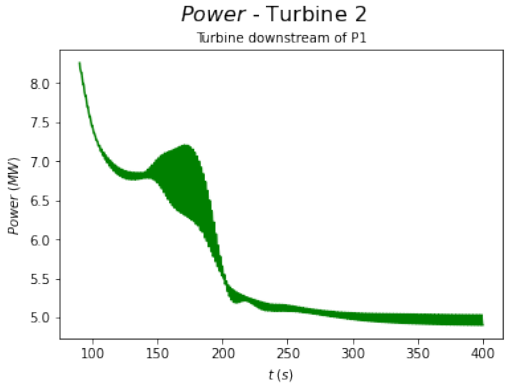

(b) Power for laminar inlet - P3

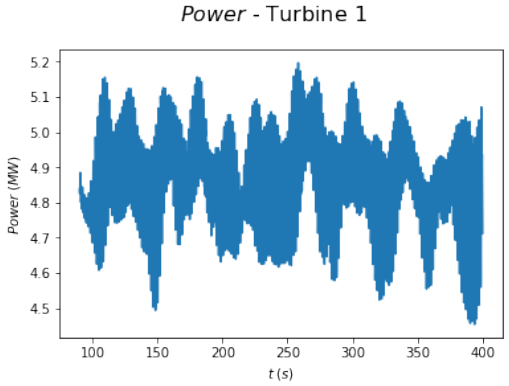

(c) Power for turbulent inlet - P1

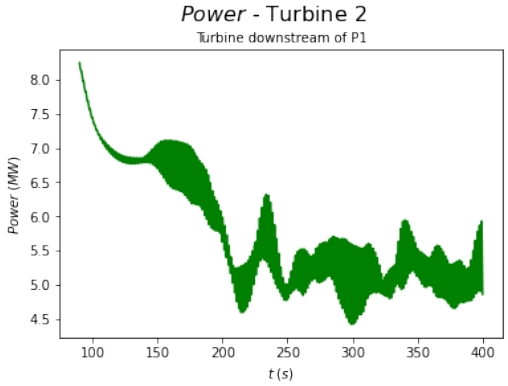

(d) Power for turbulent inlet - P3

Figure 3: Power graphs for both inlet types with the turbines in positions P1 and P3

Table 1: Turbulence comparison between different inlet types

	Turbulent Inlet				Laminar Inlet			
	Simulation P1 & P3		Simulation P3 & P4		Simulation P1 & P3		Simulation P3 & P4	
	P1	P3	P3	P4	P1	P3	P3	P4
Turbulence Intensity (%)	5.17	20.46	4.35	16.64	4.68	20.75	3.84	15.71
Turublence Kinetic Energy	0.17	2.16	0.18	1.29	0.13	2.16	0.14	1.17

develops, is similar for both inlets. However, whilst in the laminar one the power barely changes, in the turbulent one the power has several peaks, increasing the mean value significantly.

The power coefficients calculated with the wind speed obtained from the probes, shown in Fig. 4, exhibit a behaviour similar to what was described above. The turbulent inlet causes the C_p in $P1$ to decrease slightly, in average, compared to the laminar case, even though it reaches higher maximum values. For the C_p in $P3$, there is actually a significant increase of the coefficient in the turbulent condition compared to the laminar one, specially because in the final seconds of simulation the C_p grew considerably.

Table 1 shows the mean turbulence intensity (TI) and mean turbulent kinetic energy (TKE) measured 1 diameter upstream of the turbines, at hub height. Not surprisingly, $P1$ shows higher values of TI and TKE when subject to the turbulent inlet, which justifies the larger oscillations in power and C_p. However, $P3$ has a lower value for TI in the case of the turbulent inlet and an equal value for TKE for both cases. So we can infer that the higher C_p calculated using the probes is due to the faster wake recovery downstream the turbine in $P1$ present in the turbulent case, which causes an increase in the velocity upstream the rotor plane. This can be confirmed in Fig. 5, where a comparison is made for the velocities measured 1D upstream of the turbine in $P3$, for both inlet types. The plot shows a higher velocity for the turbulent inlet compared to the laminar one. Regarding the mean values, in the former it is 8.96 m/s, whilst in the latter it is 8.91m/s. This subtle difference in velocity was capable of causing a considerable increase in the C_p calculated using the probes in $P3$. Moreover, a visual assessment can be made through Fig. 6, where the velocity contour in the last simulation time step for both inlet types is compared side by side. These images were generated in the post-processing software ParaView.

We now analyse the results obtained for the second layout, where turbines are in the positions $P3$ and $P4$. Figure 7

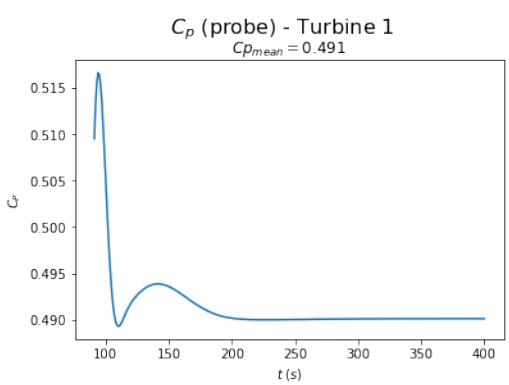

(a) C_p for laminar inlet - P1

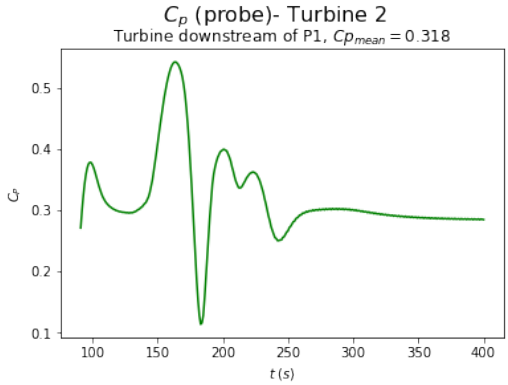

(b) C_p for laminar inlet - P3

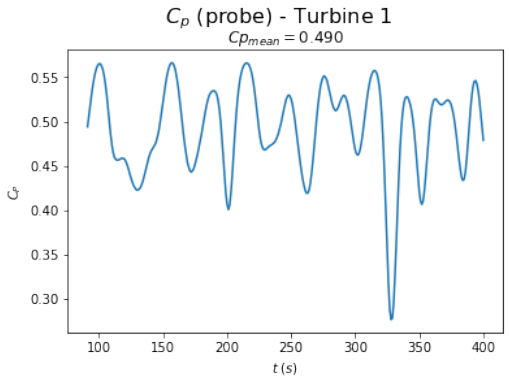

(c) C_p for turbulent inlet - P1

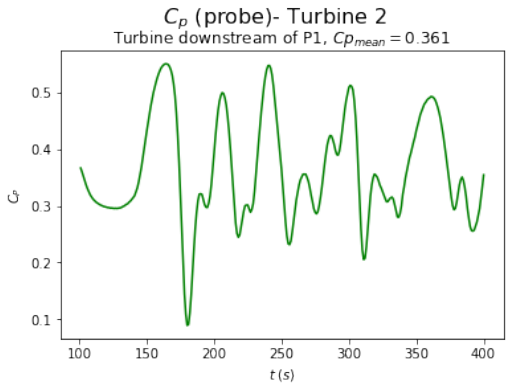

(d) C_p for turbulent inlet - P3

Figure 4: Power coefficient graphs for both inlet types with the turbines in positions P1 and P3

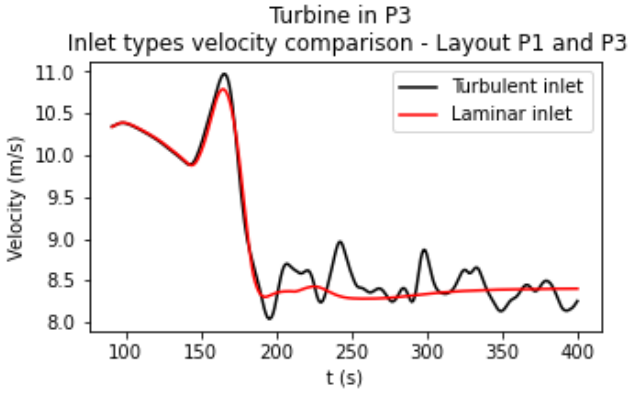

Figure 5: Velocity comparison 1 diameter upstream for the turbine P3 in the first layout (P1 and P3)

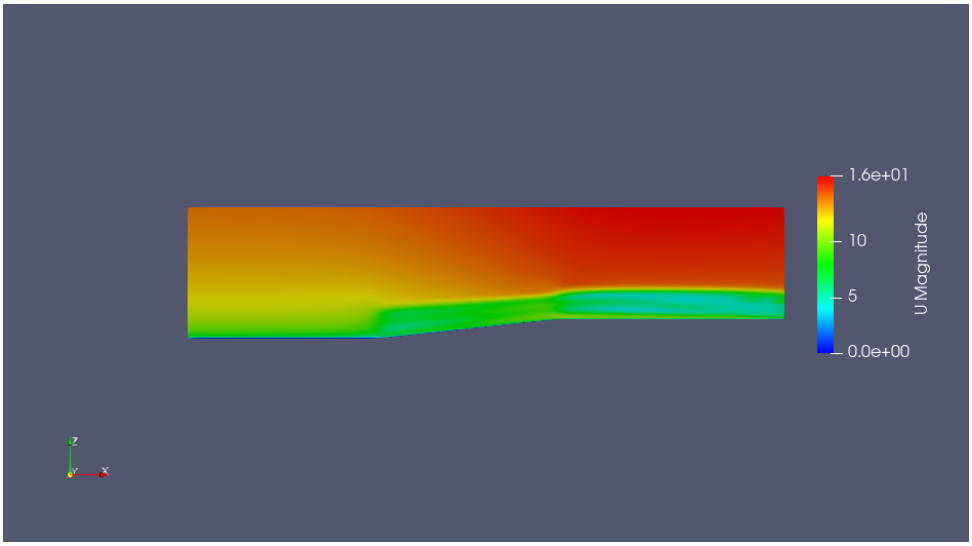

(a) Velocity contour for laminar inlet

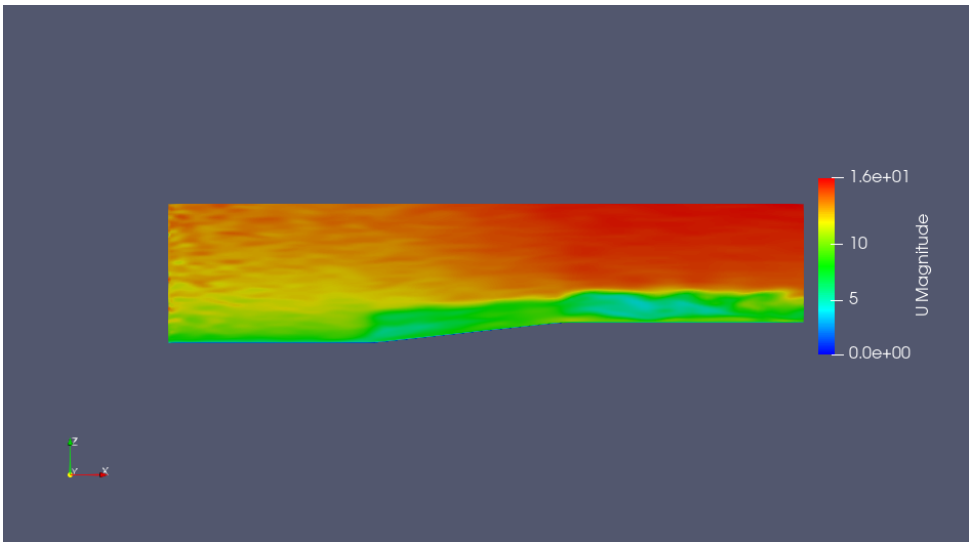

(b) Velocity contour for turbulent inlet

Figure 6: Velocity contour in the last simulation time step for both inlet types in the first layout (P1 and P3)

shows the power production for each turbine, at the different inflow conditions, and the interpretation is similar to that made for the previous layout. The main difference is the magnitude of the power, which is way above the rated value in $P3$, due to the speed up effect in the slope and because the turbine does not have a control implemented yet (otherwise, pitch control would act to limit the power to the rated value). For the turbine in $P4$, the power stabilizes at a lower value, since in this layout the turbine is completely immersed in the wake of the upstream one, $P3$.

Examining the power coefficient results, shown in Fig. 8, once again the first turbine, $P3$ in this simulation, has a slightly lower average C_p with the turbulent inlet compared to the laminar one. Also, the second one, now $P4$, has a higher C_p value in the case of turbulent inlet.

Going back to Tab. 1, it can be seen that $P3$ has both TI and TKE with larger mean values in the turbulent inlet simulation. The same occurs for the turbine in $P4$, which might be the reason why in the turbulent case the power coefficient is slightly higher compared to the laminar one. Moreover, the higher turbulence upstream generates a faster wake recovery, which is beneficial for the power production. Figure 9 shows the comparison for the velocities $1D$ upstream of the turbine in $P4$ in the second layout. Although the laminar inlet has stabilized at a higher level, several spikes occur in the turbulent inlet simulation, indicating an acceleration in the wind, which might justify the marginally superior C_p mean value in this case. Similarly to Fig. 6, the velocity contour for the second layout is show in Fig. 10.

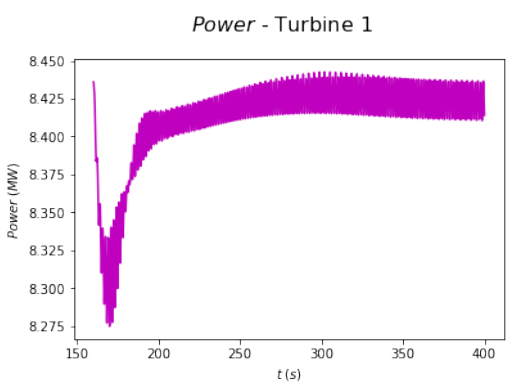

(a) Power for laminar inlet - P3

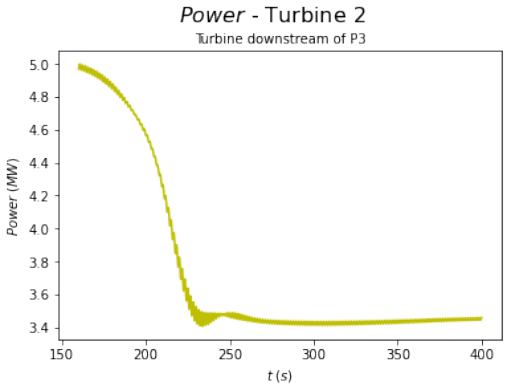

(b) Power for laminar inlet - P4

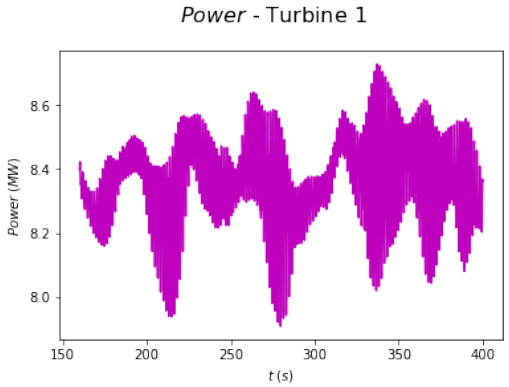

(c) Power for turbulent inlet - P3

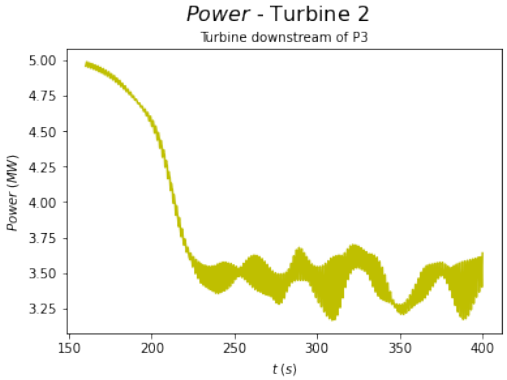

(d) Power for turbulent inlet - P4

Figure 7: Power graphs for both inlet types with the turbines in positions P3 and P4

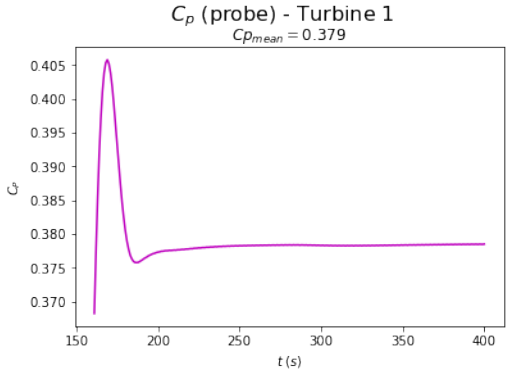

(a) C_p for laminar inlet - P3

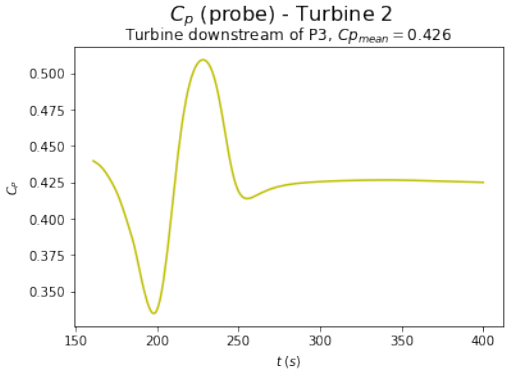

(b) C_p for laminar inlet - P4

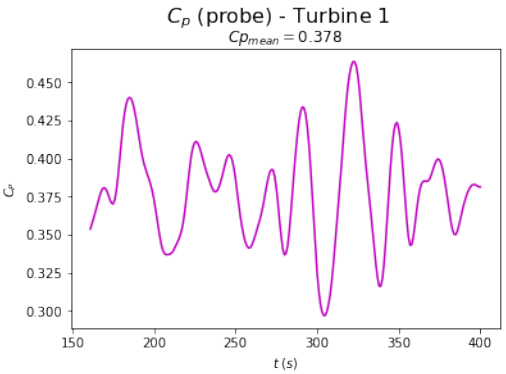

(c) C_p for turbulent inlet - P3

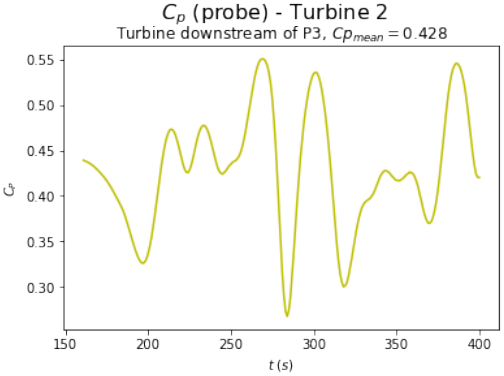

(d) C_p for turbulent inlet - P4

Figure 8: Power coefficient graphs for both inlet types with the turbines in positions P3 and P4

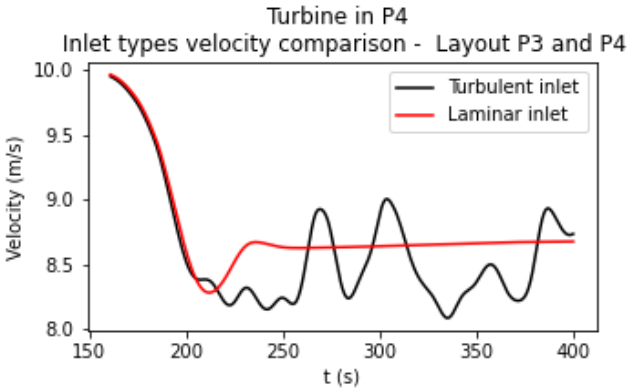

Figure 9: Velocity comparison 1 diameter upstream for the turbine P4 in the second layout (P3 and P4)

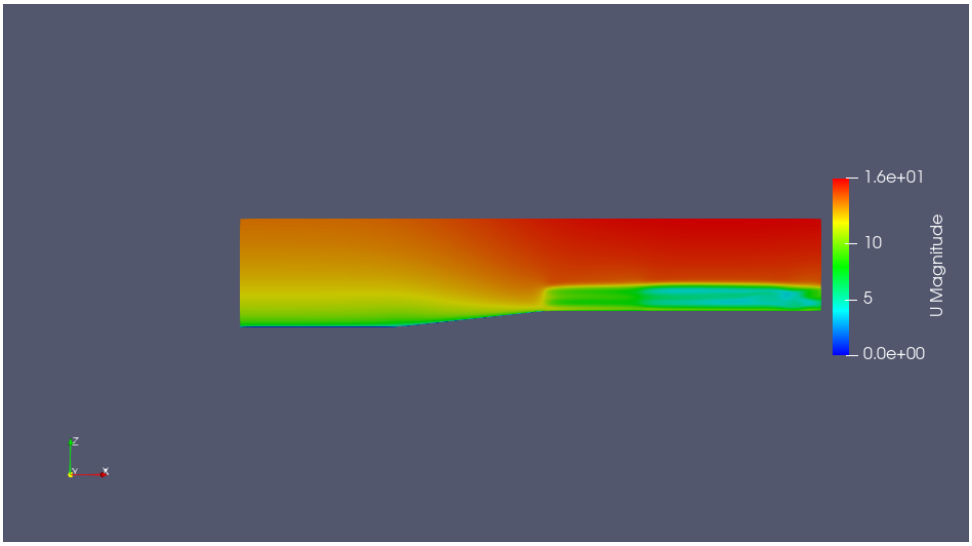

(a) Velocity contour for laminar inlet

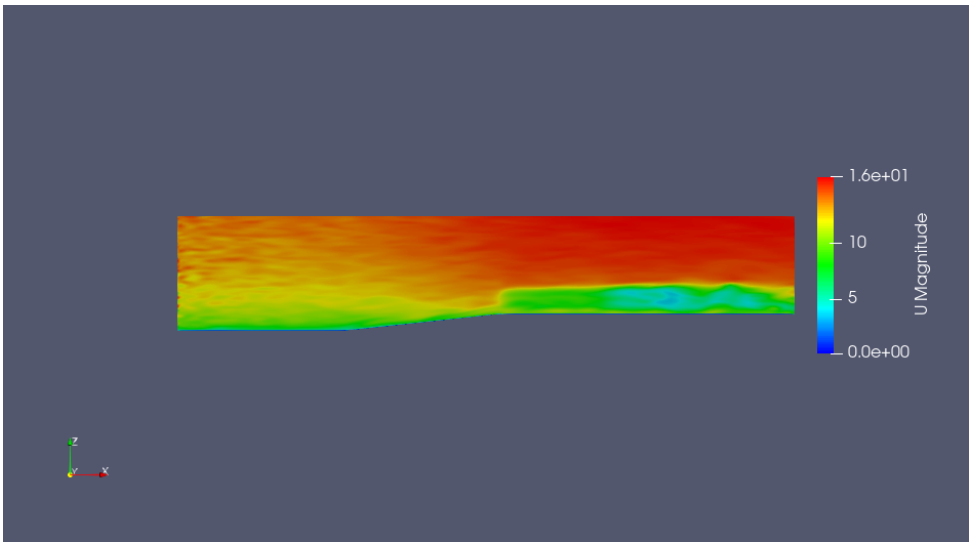

(b) Velocity contour for turbulent inlet

Figure 10: Velocity contour in the last simulation time step for both inlet types in the second layout (P3 and P4)

4. CONCLUSIONS

A comparison between two inlet types, laminar and turbulent, was carried using LES simulations employing OpenFOAM, and using the library turbinesFOAM to implement the Actuator Line Method, in an idealized complex terrain

consisting of a slope and a plateau. In order to generate the turbulence, the boundary condition DF-SEM was used. Also, two layouts were tested in the simulations with the different inlet types.

The results showed that the turbulence may decrease slightly the performance of the upstream turbine from each layout and increase the power generation for the downstream one. With respect to the first layout, the turbine in $P3$ had a higher average C_p because the increased turbulence upstream in $P1$ might have influenced in the flow downstream and caused the wake effect to recover faster, as well as the speed up effect in the slope. For the second layout, the turbine in $P4$ had a somewhat higher power coefficient in the turbulence case also due to the faster wake recovery caused by the turbulent inlet.

For future work, the rotor speed and the pitch controllers should be implemented, so that the wind turbines' power production will be limited to the rated power, increasing the fidelity of the model.

5. REFERENCES

Alfredsson, P.H. and Segalini, A., 2017. "Introduction wind farms in complex terrains: an introduction". *Phil. Trans. R. Soc. A.*, Vol. 375.

Bachant, P., 2019. "turbinesfoam". https://github.com/turbinesFoam/turbinesFoam.

Castellani, F., Astolfi, D., Mana, M., Piccioni, E., Becchetti, M. and Terzi, L., 2017. "Investigation of terrain and wake effects on the performance of wind farms in complex terrain using numerical and experimental data". *Wind Energ.*, Vol. 20.

Hansen, M.O.L., 2015. *Aerodynamics of Wind Turbines*. Routledge, 3rd edition.

Jonkman, J., Butterfield, S., Musial, W. and Scott, G., 2009. "Definition of a 5-MW Reference Wind Turbine for Offshore System Development". p. 75.

Lee, J. and Zhao, F., 2022. "Gwec | global wind report 2022". Global Wind Energy Council. 4 Apr. 2022 <https://gwec.net>.

OpenCFD, L., 2021. "Turbulence df-sem". https://www.openfoam.com/documentation/guides/latest/doc/guide-bcs-inlet-velocity-dfsem.html.

OpenCFD, L., 2022. "Openfoam". https://www.openfoam.com.

Porté-Agel, F., Bastankhah, M. and Shamsoddin, S., 2020. "Wind-turbine and wind-farm flows: A review". *Boundary-Layer Meteorol*, Vol. 174.

Sandusky, M., 2017. *Wind Farm Power Prediction In Complex Terrain*. Ph.D. thesis, Boise State University, Idaho.

Shen, W.Z., Mikkelsenand, R., Sørensen, J.N. and Bak, C., 2005. "Tip loss corrections for wind turbine computations". *Wind Energy*, Vol. 8, No. 4, pp. 457–475.

Veers, P., Dykes, K., Lantz, E. and Barth, S., 2019. "Grand challenges in the science of wind energy". *Science 366*, Vol. eaau2027.

6. RESPONSIBILITY NOTICE

The authors are the only responsible for the printed material included in this paper.